Mineralogy and Petrology (2025) 119:279–287
https://doi.org/10.1007/s00710-025-00936-y

RESEARCH

Three columbite-group minerals from Ratnapura, Sri Lanka

K. A. Geeth Sameera[1,2] · Chutimun Chanmuang N.[1] · Radek Škoda[3] · Manfred Wildner[1] · Lutz Nasdala[1]

Received: 12 December 2024 / Accepted: 23 May 2025 / Published online: 2 July 2025

Abstract
Three oxide minerals belonging to the columbite group, including columbite–(Mn) ($MnNb_2O_6$), columbite–(Fe) ($FeNb_2O_6$), and fersmite ($CaNb_2O_6$), were found in specimens from gem placers in Ratnapura district, Sri Lanka. We present results of chemical, structural and spectroscopic analyses, including the first Raman spectrum for natural fersmite. For columbite–(Mn) and columbite–(Fe), analytical results obtained before and after dry annealing in air indicate low degrees of accumulated self-irradiation damage, which corresponds well with low actinide concentrations.

Keywords Columbite–(Mn) · Columbite–(Fe) · Fersmite · EPMA chemical analysis · Single-crystal X-ray diffraction · Raman spectroscopy

Introduction

The minerals columbite–(Mn), $MnNb_2O_6$, columbite–(Fe), $FeNb_2O_6$, and fersmite, $CaNb_2O_6$, are orthorhombic (space group *Pbcn*; Hess and Trumpour 1959; Wenger et al. 1991; Tarantino and Zema 2005). They are members of the columbite group, which in turn belongs to the columbite supergroup (Chukanov et al. 2023). Columbite–(Fe) forms a solid solution with columbite–(Mn). The latter has wide Nb-Ta miscibility and forms a solid solution with tantalite–(Mn), $MnTa_2O_6$ (Ercit et al. 1995). In contrast, there is no complete solid solution with, but an extended two-phase region towards $FeTa_2O_6$, which prefers the tetragonal trirutile (tapiolite) structure (Černý et al. 1992; Ercit et al. 1995). The columbite structure can–greatly simplified– be derived from the ixiolite-type unit cell [$(A,B)O_2$] by triplication along the *a* axis resulting from cation ordering [AB_2O_6] (Chukanov et al. 2023). Among columbite-group minerals, a structural peculiarity of fersmite is that the A site, occupied by the comparably large Ca^{2+}, is 8-coordinated, whereas Mn^{2+} in columbite–(Mn) and Fe^{2+} in columbite–(Fe) are sixfold coordinated. Fersmite is dimorphous with the aeschynite-group mineral vigezzite, $CaNb_2O_6$, whose structure has been described in the orthorhombic space group *Pnmb* (Giuseppetti and Tadini 1990).

Prior to the introduction and international acceptance of suffix terminology for minerals that are group members (Burke 2008), columbite–(Mn) was named manganocolumbite and columbite–(Fe) was named ferrocolumbite, referring to the dominating A-site cation and the relationship to other mineral species of the columbite group. The term columbite, in turn, goes back to “columbium”, an ancient name for the element Nb (named by Hatchett 1802; after the discoverer of America, Christophorus Columbus). Columbite-group minerals typically occur in–often highly fractionated–granites and granitic pegmatites (Kristiansen 1994; Baumgartner et al. 2006; Linnen et al. 2012; Melcher et al. 2015; Feng et al. 2020).

The discovery of Sri Lankan columbite–(Mn) actually goes back to the 1990s, when a dark pebble (ca. 32 g; $2.8 \times 2.3 \times 1.6$ cm^3) was found in the heavy-mineral fraction–often referred to as “*katta*”– derived from an eluvial gem mine in the Karapincha-Paradise area in Kuruwita, located about 9 km north-northwest of Ratnapura. The

Editorial handling: K. Randive

K. A. Geeth Sameera
sameera.kasthuri.arachchige@univie.ac.at

Chutimun Chanmuang N.
chutimun.chanmuang@univie.ac.at

1 Institut für Mineralogie und Kristallographie, Universität Wien, Josef- Holaubek-Platz 2, Wien A–1090, Austria

2 Geological Survey and Mines Bureau, 569 Epitamulla road, Pitakotte 10100, Sri Lanka

3 Department of Geological Sciences, Faculty of Science, Masaryk University, Kotlářská 267/2, Brno 61137, Czech Republic

specimen (Fig. 1a) had a water-worn shape. Initially the pebble was believed to consist of thorianite. It was sent by the owner for identification to the Department of Geology and Geophysics, Rice University, Houston, Texas. There it was subjected to chemical analysis using a CAMECA SX50 instrument (15 kV; 15 nA). Complete analytical details cannot be retraced anymore. In the mineral identification report (issued on 2 November 1998 by electron microprobe technician Milton L. Pierson), the mineral was identified as “mildly radioactive manganocolumbite”. Also, it was stated that observation under the optical microscope did not reveal any inclusions or features that would indicate a synthetic origin for the stone. The report, however, remained undisclosed to the public. In the meantime, the sample was cut into three pieces that were then ground and polished as gemmy cabochons (Fig. 1b).

Much more recently, in 2021, another pebble of similar appearance (Fig. 1c) was collected from “*katta*” in a placer gem mine in Dodampe, 9 km northwest of Ratnapura. This dark grey to black sample had an irregular to rounded shape and weighed about 11 g ($2.8 \times 2.0 \times 0.5$ cm^3 size). Preliminary spectroscopic analyses indicated a columbite-group mineral as well.

To the best of our knowledge, there is no mention in the literature or on the internet of any occurrence of columbite-group minerals in Sri Lanka. We have therefore revisited the Kuruwita specimen, and also included the Dodampe pebble, in a combined electron probe micro-analyser (EPMA), single-crystal X-ray diffraction and Raman spectroscopic study. Results are presented in the present brief report.

Materials and methods

From both samples under investigation, large specimens (one cabochon made from the Kuruwita specimen, and the initial Dodampe specimen) were provided to us on loan by the owners, for taking photographs and determination of the specific gravity (SG). This parameter was measured hydrostatically, by weighing samples in distilled water (to reduce surface tension, a drop of detergent was added) and in air. The procedure was repeated three times.

In addition, we received a few large fragments (several mm size) per sample for analysis. To reconstitute structural disturbance– possibly due to primary incorporation of non-formula constituents, primary cation disorder, and/or secondary self-irradiation damage– two small chips of each sample were subjected to annealing in air at 1100 °C for 48 h (for further details of the procedure see Erlacher et al. 2021). Both un-annealed and annealed chips were then embedded in araldite epoxy, with random orientation, and ground and polished to reveal internal features. Prior to back-scattered electron (BSE) imaging and EPMA chemical analysis, the sample mount was coated with carbon for electric conductivity.

Reflected-light images of polished grains were taken using a Keyence VHX-7100 digital microscope. Back-scattered electron images of un-annealed fragments were obtained in a Tescan Vega 4 scanning electron microscope (SEM), at 15 kV and 10 nA. With the same SEM, qualitative X-ray element-distribution maps were obtained at 20 kV and 6 nA, using an Oxford instruments Xplore30 energy-dispersive detector.

Chemical analyses by means of wavelength-dispersive X-ray spectrometry were conducted using a CAMECA SX100 EPMA. The system was operated at 15 kV and 20 nA, and the focal-spot diameter of the electron beam was 5 µm. Synthetic and natural reference materials used for calibration included the following (analysed X-ray lines and peak counting times are quoted in brackets; background counting times were half of the respective peak counting time): topaz (F*K*α; 40 s), albite (Na*K*α; 20 s), Mg_2SiO_4 (Mg*K*α; 40 s), almandine (Al*K*α and Si*K*α; 40 s); wollastonite (Ca*K*α; 20 s), anatase (Ti*K*α; 20 s), $ScVO_4$ (Sc*K*α; 40 s), Mn_2SiO_4 (Mn*K*α; 20 s), columbite–(Fe) from Ivigtut (Fe*K*α and Nb*L*α; 20 s), gahnite (Zn*K*α; 40 s), YAG (Y*L*α; 40 s),

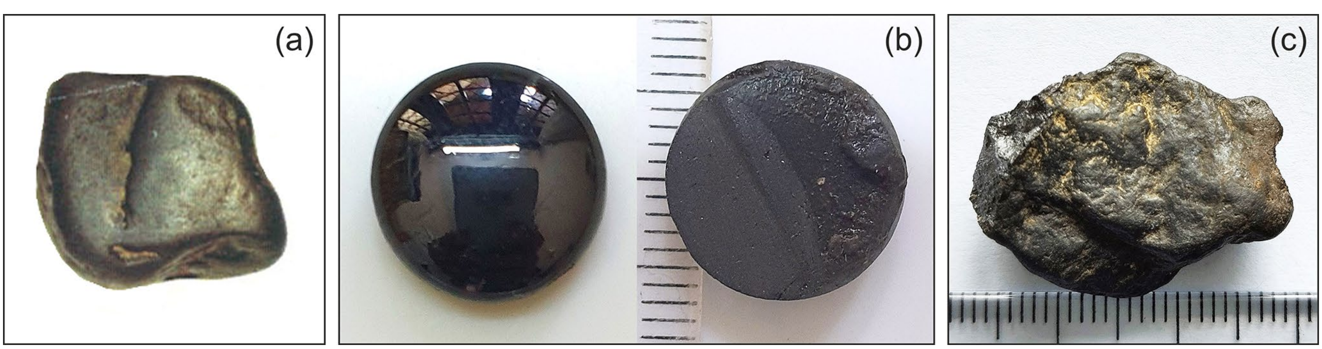

Fig. 1 (**a**) This low-quality image was scanned from the 1998 report of Rice University. It is the only still available picture of the original Kuruwita specimen (largest dimension 2.8 cm). (**b**) Two photographs showing the polished front and the unpolished rear side of one of the cabochons (ca. 11 ct) produced from the Kuruwita specimen. (**c**) Photograph of the original Dodampe specimen

zircon (Zr$L\alpha$; 40 s), Sn metal (Sn$L\alpha$; 40 s), Sb metal (Sb$L\beta$; 40 s), $CrTa_2O_6$ (Ta$M\alpha$; 20 s), $CaWO_4$ (W$L\alpha$; 40 s), anglesite (Pb$M\alpha$; 40 s), Bi metal (Bi$M\beta$; 40 s), ThO_2 (Th$M\alpha$; 40 s) and U metal (U$M\beta$; 40 s). Matrix correction was made using the XPhi routine (Merlet 1994), and detection limits (Table 1) were calculated using the Peaksight software provided by CAMECA, which is based on Ziebold (1967). For further EPMA experimental details, readers are referred to Loun et al. (2018).

Unit-cell parameters of un-annealed and annealed columbite–(Mn) and columbite–(Fe) were determined at 23 °C on a Nonius KappaCCD single-crystal X-ray diffractometer with charge-coupled device (CCD) area detector using graphite-monochromatised Mo$K\alpha$ radiation. The data were extracted from full-sphere data collections up to 80° 2θ, and refined using the program DENZO-SMN (Nonius 1998).

Raman spectra (un-annealed and annealed chips) and hyperspectral Raman maps [un-annealed chips of columbite–(Fe) only] were obtained using a Horiba LabRAM HR Evolution spectrometer equipped with Olympus BX-series microscope, a grating with 1800 grooves per mm in the optical pathway, Peltier-cooled CCD detector and software-controlled x-y(-z) sample stage. Spectra were excited with the 632.8 nm emission of a He-Ne laser (10 mW at the sample surface). The laser light was focused, and the scattered light was collected, with a 50× objective (numerical aperture 0.55). A 100× objective was not used, in order to decrease the laser-power density across the focal-spot area (to avoid thermal decomposition of the analysed area) without the need to decrease the absolute laser power. The Rayleigh line was used to do wavenumber calibration. The spectral resolution was ca. 0.8 cm^{-1}. For further details see Zeug et al. (2018).

Results and discussion

General characterisation

Specific gravities of the natural samples, herein reported as mass densities, were determined at 6.00 ± 0.01 g/cm^3 (Kuruwita specimen) and 6.22 ± 0.01 g/cm^3 (Dodampe specimen). Reflected-light and BSE images are presented in Fig. 2. The Kuruwita sample (Fig. 2a) appears widely homogeneous. The Dodampe specimen (Fig. 2b–d), in contrast, shows distinct zoning and heterogeneity. Some grains consist of two domains that differ significantly in terms of their BSE intensity; both of them show notable internal zoning. In contrast to the Kuruwita sample, the Dodampe specimen is intergrown with porous patches of another mineral (which is identified as the columbite-group mineral fersmite; see below). Also, the Dodampe specimen is fairly rich in small inclusions and voids. Inclusions, identified by Raman spectroscopy, are predominantly rutile and rarely idiomorphic zircon.

Chemical composition

Results of EPMA chemical analyses are presented in Table 1. The Kuruwita sample is columbite–(Mn) with the mean chemical formula:

Table 1 Mean chemical compositions (EPMA results; wt%) of the three columbite-group minerals

	Kuruwita sample:	Dodampe sample:			Detection limit
	Columbite–(Mn)	Columbite–(Fe) (bright BSE)	Columbite–(Fe) (dark BSE)	Fersmite	
Constituent*	(n=8)	(n=11)	(n=6)	(n=2)	
F	bdl	bdl	bdl	0.37 ± 0.01	0.05
MgO	bdl	bdl	0.10 ± 0.04	bdl	0.03
SiO_2	bdl	bdl	bdl	0.38 ± 0.04	0.07
CaO	bdl	bdl	bdl	13.43 ± 0.13	0.05
TiO_2	0.87 ± 0.02	0.92 ± 0.09	1.78 ± 0.48	1.31 ± 0.06	0.07
MnO	13.64 ± 0.10	6.97 ± 0.13	6.57 ± 1.28	0.50 ± 0.23	0.06
FeO	4.53 ± 0.04	10.81 ± 0.29	12.08 ± 1.14	0.36 ± 0.07	0.07
ZrO_2	0.23 ± 0.03	0.30 ± 0.05	0.15 ± 0.09	0.23 ± 0.04	0.12
Nb_2O_5	49.64 ± 0.13	42.81 ± 3.52	51.22 ± 21.87	36.57 ± 0.28	0.14
Ta_2O_5	30.20 ± 0.24	37.90 ± 3.52	27.91 ± 1.47	44.28 ± 0.17	0.11
WO_3	0.31 ± 0.18	bdl	bdl	bdl	0.16
UO_2	0.29 ± 0.12	bdl	bdl	bdl	0.24
Total	99.75	99.82	99.95	97.59	

Notes: All errors are quoted at the 2s level. Na (0.05), Al (0.03), Sc (0.06), Zn (0.14), Y (0.09), Sn (0.08), Sb (0.27), Bi (0.18) and Th (0.12) were analysed as well and yielded means below the respective detection limit (values in brackets; in wt%) in all phases. BSE images with EPMA analysis points are provided in the ESM

* Total Mn is quoted as MnO and total Fe is quoted as FeO

bdl = mean below the respective EPMA detection limit

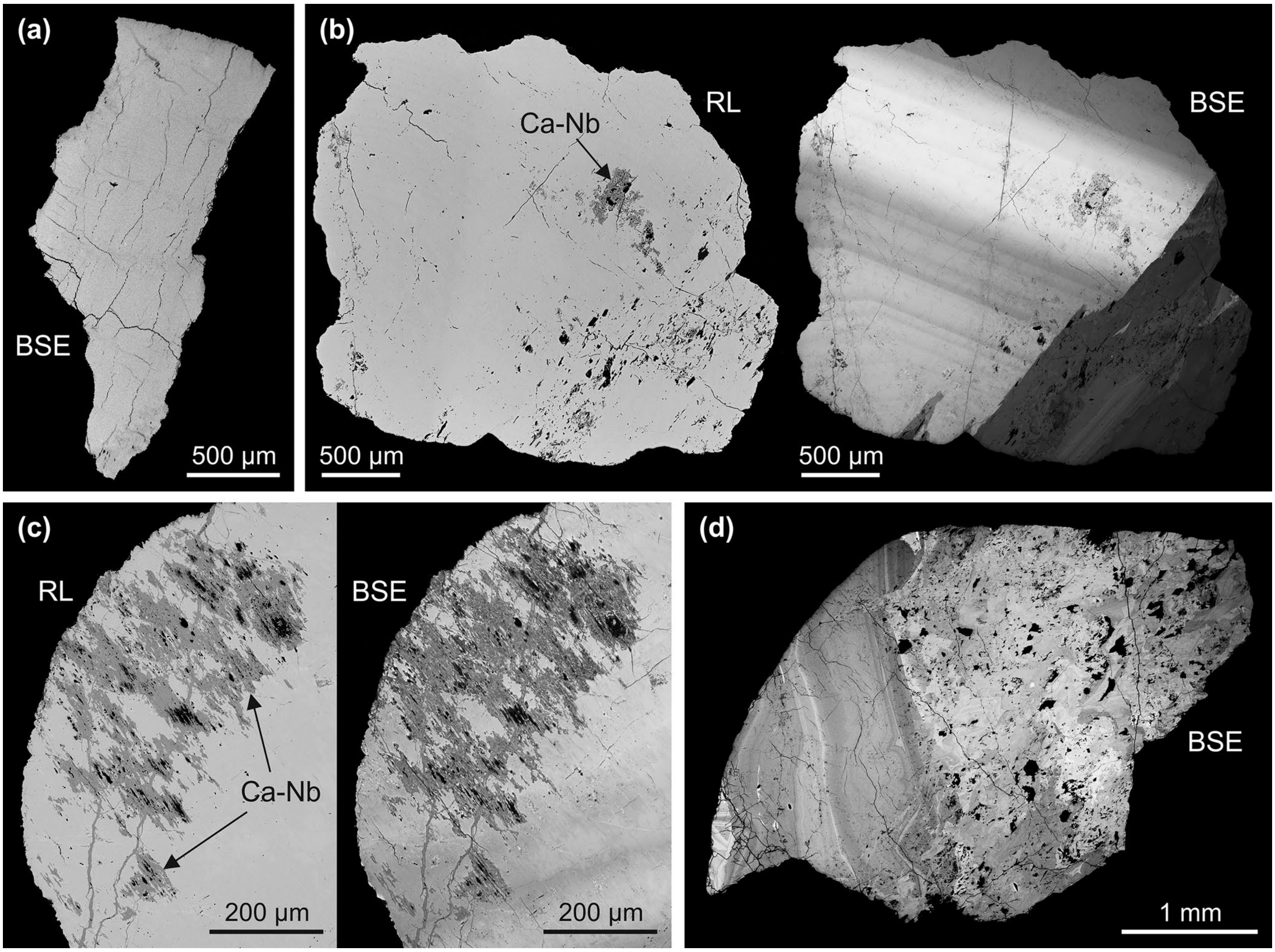

Fig. 2 Reflected light (RL) and BSE photomicrographs of polished grains of the two samples. (**a**) The Kuruwita sample yielded fairly uniform BSE intensity. (**b**) In reflected light, this grain of the Dodampe sample shows irregular patches of a lower-reflectance Ca-Nb phase (arrow) and numerous tiny inclusions and pores. The apparently homogeneous host phase reveals strong zoning when observed in BSE mode. Note that both the upper left, bright-BSE domain (showing straight growth banding) and the lower right, dark-BSE domain (showing rather complex zoning) are columbite–(Fe). (**c**) Pair of images of another bright-BSE columbite–(Fe) grain from Dodampe containing a large bunch of irregularly shaped patches of the (strongly porous) Ca-Nb phase. (**d**) BSE image of another columbite–(Fe) grain from Dodampe, revealing complex internal zoning and heterogeneity, and the extensive presence of inclusions and pores (both are seen as black patches). Samples shown in **a** and **b** were analysed by EPMA; images with marked locations of analysis spots are provided in the electronic supplementary material (ESM)

$$(Mn_{0.74}Fe_{0.24}Zr_{0.01})\,(Nb_{1.43}Ta_{0.52}Ti_{0.04})\,O_6$$

(calculated based on the assumption of 6 O atoms per formula unit). Variations among individual analysis results are small (Fig. 3), supporting the material's homogeneity. In accordance to its heterogeneous appearance, the Dodampe sample yielded varying chemical compositions; nevertheless both of the major domains belong to columbite–(Fe) (see also Fig. 3):

$$(Fe_{0.60}Mn_{0.39}Zr_{0.01})\,(Nb_{1.27}Ta_{0.68}Ti_{0.05})\,O_6\ \text{(bright - BSE domain)}$$
$$(Fe_{0.63}Mn_{0.35}Zr_{0.01}Mg_{0.01})\,(Nb_{1.45}Ta_{0.48}Ti_{0.08})\,O_6\ \text{(dark - BSE domain).}$$

Bright- and dark-BSE domains differ predominantly in their Nb/Ta ratios (Fig. 3). Zoning within the dark-BSE domain is driven by variable Mn/Fe ratios whereas the bright-BSE domain is fairly uniform in Mn/Fe but has significant variation in Nb/Ta that correlate with the BSE intensity. The latter observation explains BSE differences as $\overline{Z}$ (average atomic number) contrast (compare Hall and Lloyd 1981): Elevated amounts of Ta accompanied by lower amounts of Nb lead to higher $\overline{Z}$ and, with that, increased η (back-scatter coefficient; fraction of primary electrons that are deflected through an angle of >90°) due to the higher number of charge carriers of higher-*Z* elements (Donovan et al. 2003).

Mulja et al. (1996) found that in pegmatitic columbite-group species, Ta/(Ta+Nb) and Mn/(Mn+Fe) correlate

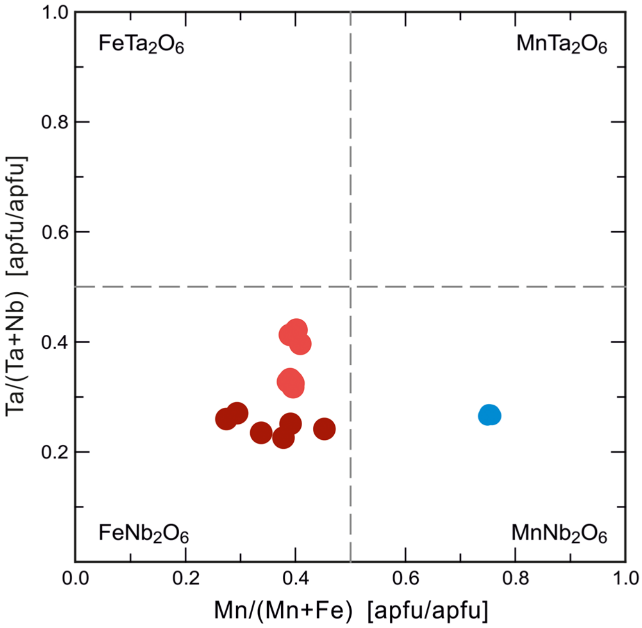

Fig. 3 Compositions of the Kuruwita and Dodample specimens. Blue, columbite–(Mn) ($n=8$); dark red, dark-BSE columbite–(Fe) ($n=6$); bright red, bright-BSE columbite–(Fe) ($n=11$)

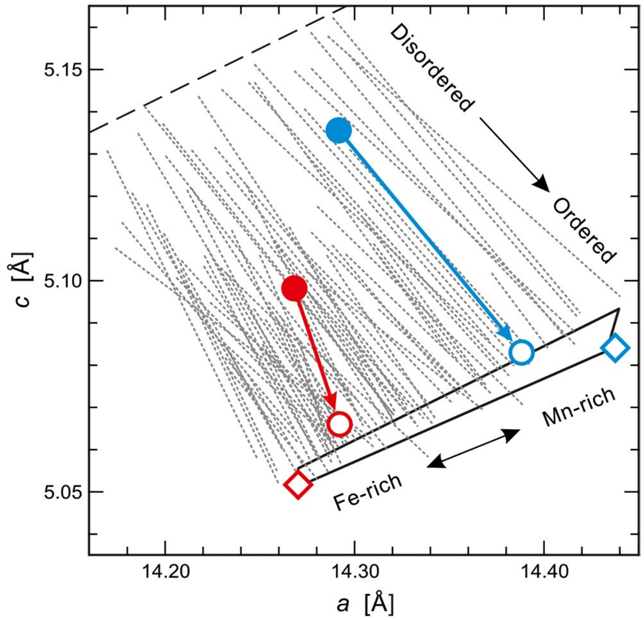

Fig. 4 Plot of unit-cell parameters c versus a. (redrawn after Ercit et al. 1995), visualising parameter changes upon annealing-induced cation ordering. The dashed line at the top represents the anticipated upper limit for (fully) disordered samples, and dotted lines represent heating paths for unheated and heated pairs, with unheated samples plotting at the upper left end of each path and heated samples at the lower right end (both from Ercit et al. 1995). Blue circles, columbite–(Mn) from Kuruwita; red circles, columbite–(Fe) from Dodampe. Full circles, natural samples; open circles, annealed samples. Analogously coloured diamond symbols represent unit-cell parameters of synthetic, fully ordered end-members (Tealdi et al. 2004)

Table 2 Unit-cell parameters (determined by single-crystal X-ray diffraction)

Sample	a (Å)	b (Å)	c (Å)	V (Å^3)
Columbite–(Mn)	14.292(4)	5.749(2)	5.136(1)	421.93(24)
Columbite–(Mn); annealed	14.388(3)	5.755(1)	5.083(1)	420.92(15)
Columbite–(Fe)	14.297(3)	5.740(1)	5.094(1)	418.09(21)
Columbite–(Fe); annealed	14.292(3)	5.736(1)	5.066(1)	415.34(15)

Note: Errors are quoted at the 2s level

positively with the degree of pegmatite evolution. However, pegmatitic evolution does not seem to be the only feature in control of the chemical composition of columbite–(Fe): In the Dodampe sample, the highest-Ta growth zone (brightest-BSE zone in Fig. 2b) is sandwiched between lower-Ta growth zones, and these are discordantly overgrown by a low-BSE domain with even lower Ta/(Ta+Nb).

Single-crystal X-ray diffraction studies of Mn-Fe columbites

Single-crystal X-ray analyses of un-annealed and annealed chips of the two samples validated the orthorhombic space group *Pbcn*. Unit-cell parameters are listed in Table 2. Both samples experienced comparably moderate, annealing-induced volume shrinking of the unit cell, with somewhat deviating trends that nevertheless correspond well with earlier observations (Fig. 4; Ercit et al. 1995; Mulja et al. 1996; Balassone et al. 2015). The size of unit cell of columbite–(Mn) was reduced by only 0.24 vol%, caused by expansion along c and contraction along a (with insignificant change of parameter b). The unit cell of columbite–(Fe) shrank by 0.66 vol%, mainly because of reduction along c. For both samples, the decidedly minor volume decrease upon annealing indicates that (i) samples were affected by moderate (primary) cation disorder and (ii) specimens had stored, if at all, only minor amounts of radiation damage. This is also supported by the observation of fairly sharp X-ray diffraction maxima. The more significant c versus a change of the columbite–(Mn) (Fig. 4) points to a higher extent of initial cation disorder (that is, Mn at the Nb site and vice versa) in this sample (compare Ercit et al. 1995; Balassone et al. 2015).

Raman spectroscopy of Mn–Fe columbites

Raman spectra of columbite–(Mn) and columbite–(Fe) are presented in Fig. 5. The general fingerprints are similar to each other – both are dominated by a main band at around 877 cm^{-1}– and correspond reasonably well with published spectra of natural "manganocolumbite" (Moreira et al. 2010a), synthetic $MnNb_2O_6$ (Husson et al. 1977a) and

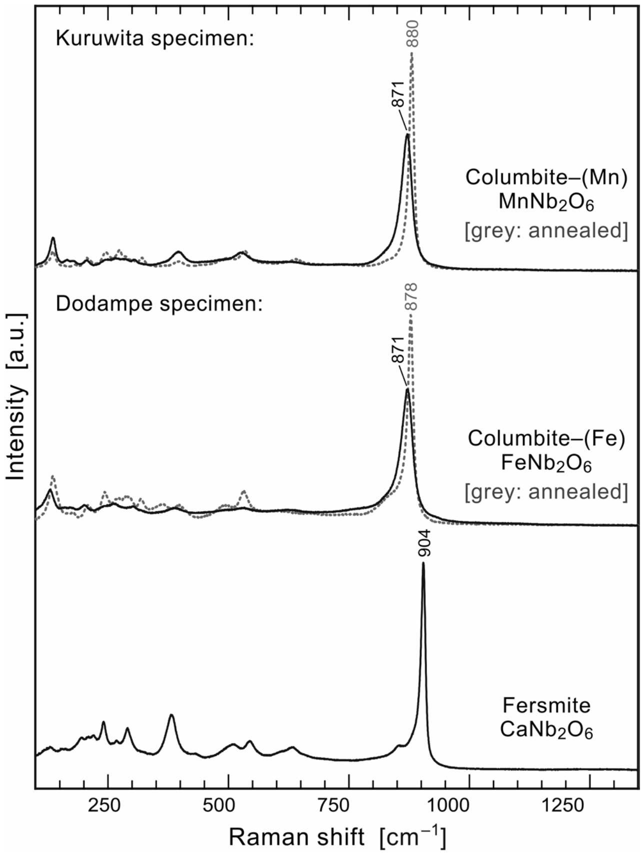

Fig. 5 Raman spectra of the three columbite-group minerals. For columbite–(Mn) and columbite–(Fe), a spectrum after annealing at 1100 °C (dotted, grey) is shown in addition. Spectra are shown with vertical offset for clarity. Note that differences in relative band intensities are due to random sample orientations with respect to laser-light polarisation

synthetic $FeNb_2O_6$ (Kumari et al. 2014), respectively. However, whereas the columbite–(Mn) yielded widely uniform spectra, the Raman spectra obtained from columbite–(Fe) showed moderate differences in band position and broadening. This observation seems to correspond to the observation of nearly uniform BSE of columbite–(Mn) but heterogeneous BSE of columbite–(Fe), and to the more extensive chemical variations of the latter (Table 1).

The main Raman band of columbite–(Mn) was described to have a Raman shift of ca. 880 cm^{-1} (877 cm^{-1} according to Husson et al. 1977a; and 882 cm^{-1} according to Moreira et al. 2010a). It is relatively narrow with a full width at half maximum (FWHM) of ca. 12 cm^{-1} (Moreira et al. 2010a). This band is assigned to symmetric stretching vibrations (A_g mode) of NbO_6 polyhedrons (Husson et al. 1977b). In a study of variably radiation-damaged columbite–(Mn) from rare-metal pegmatites in Xinjiang, China, Hao et al. (2023) found that at elevated stages of radiation-damage accumulation, the main A_g band of this mineral shifts down to <855 cm^{-1} and broadens considerably (FWHM > 50 cm^{-1}).

We obtained the main Raman band of the Kuruwita columbite–(Mn) at 871 cm^{-1} (FWHM 22 cm^{-1}). In spite of potentially significant effects of the chemical composition on Raman spectra (especially "chemical band broadening"; see for instance Ruschel et al. 2012), our spectrum points to rather moderate structural disorder and hence a fairly low degree of radiation damage, thus supporting the single-crystal X-ray results. This is also confirmed by the observation of moderate sharpening of the Raman spectrum upon annealing/heating; the main A_g band is now at 880 cm^{-1} (FWHM 11 cm^{-1}). In addition, it needs to be considered that not all structural disorder in the un-annealed sample can be assigned to radiation damage. It is well known that cation disorder (which is also reduced or even eliminated upon annealing at 950–1000 °C or above; dos Santos et al. 2001) may affect notably the unit-cell parameters of columbite-group minerals (Ercit et al. 1995; Balassone et al. 2015). Analogous effects of cation order/disorder on the Raman spectrum of columbite-group minerals have, to the best of our knowledge, not been studied thus far.

We are not aware of any detailed Raman study of columbite–(Fe), therefore we merely present our spectroscopic results without the option to discuss them considering the literature. For columbite–(Fe), we observed the main band at 869–872 cm^{-1} (FWHM 22–25 cm^{-1}) before and 878 cm^{-1} (FWHM 17 cm^{-1}) after annealing. The significantly lower difference between data for un-annealed sample and its annealed counterpart, compared to that of the Kuruwita sample, indicate an even lower degree of structural disturbance (primary cation disorder and/or secondary radiation damage) in the Dodampe sample, which is also supported by particularly low U and Th contents below the EPMA detection limits (Table 1). It is interesting to note that the larger FWHM observed after annealing seems to indicate more extensive "chemical band broadening" (Ruschel et al. 2012), compared to the columbite–(Mn) sample, in spite of rather similar contents of non-formula elements. On the other hand, the observation may also be caused by the annealed chip's random orientation in the mount: Moreira et al. (2010a) found the FWHM of the main Raman band to depend notably on crystal orientation with respect to the polarisation of the laser beam. A detailed explanation of the (apparent or actual?) higher FWHM of the annealed Dodampe columbite–(Fe) cannot be given at the present state.

The discovery of fersmite

Few EPMA analyses of the patchy phase within the Dodampe columbite–(Fe) (Table 1) yielded a Ca-Nb oxide [approximately $(Ca_{0.96}Mn_{0.03}Fe_{0.02}Zr_{0.01})$ $(Nb_{1.10}Ta_{0.80})$ O_6 with traces of Si and F]. The chemical composition appears

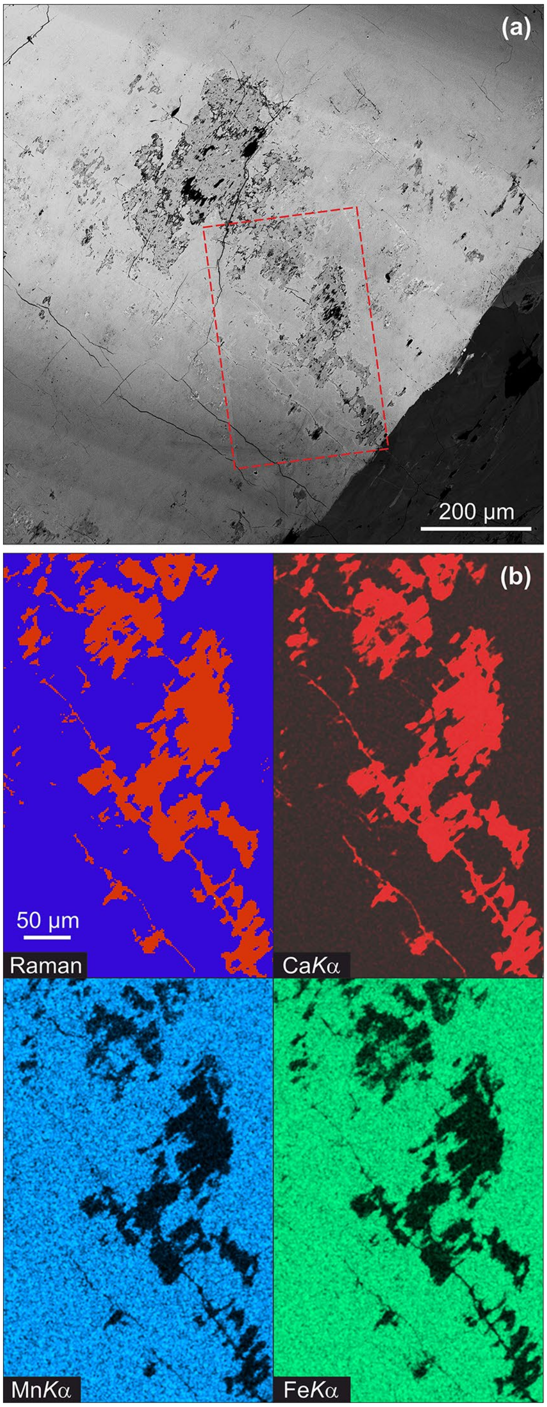

Fig. 6 Distribution of fersmite in columbite–(Fe) from Dodampe. (**a**) Detail enlargement of the BSE image shown in Fig. 2b. The red rectangle marks the area subjected to mappings. (**b**) Array of Raman and three X-ray maps. The hyperspectral Raman map ($291 \times 185 = 53835$ analyses; step width 1.5 µm) shows colour-coded the 904 cm^{-1} / 871 cm^{-1} band intensity ratio. Red ($\gg$1) = fersmite; blue ($\ll$1) = host columbite–(Fe)

to correspond to that of the dimorphous $CaNb_2O_6$ minerals fersmite and vigezzite. This porous phase (Fig. 2c) emanates from fractures in the columbite–(Fe) (Fig. 6). It therefore seems to be the product of (Fe, Mn) → Ca replacement upon secondary, fluid driven alteration of the primary host columbite–(Fe).

The Raman spectrum of the $CaNb_2O_6$ phase it shown in Fig. 5. It is similar to the principal band patterns of columbite–(Mn) and columbite–(Fe), with somewhat higher Raman shifts; the comparably narrow (FWHM 10 cm^{-1}) main band lies at 904 cm^{-1}. Identification of this spectrum was not straightforward, as it does not match with the reference spectra of both of the dimorphous $CaNb_2O_6$ minerals (fersmite and vigezzite) in the RRUFF database (https://rruff.info/; accessed 08 November 2024). However, we found that the RRUFF entry for fersmite (file R060717 containing the remark "identification of this mineral is not yet confirmed") is incorrect; it rather seems to belong to a Mn-Fe columbite. Our spectrum (Fig. 5) corresponds to published Raman spectra of the synthetic analogue of fersmite, that is, *Pbcn*-structured $CaNb_2O_6$ (Husson et al. 1977a; Moreira et al. 2010b), allowing us to identify the Ca-Nb phase inside the Dodampe columbite–(Fe) as the columbite-group mineral fersmite.

Conclusions

Dark heavy minerals recovered as by-products in Sri Lankan gem mines do not receive much attention. The present and other recent studies of such species has led to the discovery of minerals from Sri Lanka that either were merely mentioned in earlier publications but have never been properly studied (Prame et al. 2014; Erlacher et al. 2021; Nasdala et al. 2023), or minerals that were fully unknown thus far to occur in Sri Lanka (present study). It appears most worthwhile to subject especially the heavy-mineral fraction in "*katta*", but also similar species originating from pegmatites and other primary sources, to more detailed investigation. A project addressing this topic will be undertaken during the next four years, as co-operation between University of Vienna, Austria, and the Geological Survey and Mines Bureau, Sri Jayawardenepura Kotte, Sri Lanka.

Supplementary Information The online version contains supplementary material available at https://doi.org/10.1007/s00710-025-00936-y.

Acknowledgements Winston S. Molligoda (Kuruwita specimen) and G.D. Nandana Edirisinghe (Dodampe specimen) are sincerely thanked for loaning specimens for taking photographs and SG determination, and for providing sample material for analysis. Sample preparation was done by Andreas Wagner. Export permission for samples was provided by the Geological Survey and Mines Bureau, Sri Jayawardenepura Kotte, Sri Lanka. Constructive reviews by two anonymous experts and editorial handling by Kirtikumar R. Randive are gratefully acknowledged.

Funding Open access funding provided by University of Vienna.

References

Balassone G, Danisi RM, Armbruster T, Altomare A, Moliterni AG, Petti C, Mondillo N, Ghiara MR, Saviano M (2015) An insight into crystal chemistry and cation order of columbite-(Fe) and columbite-(Mn) from worldwide occurrences. N Jb Min Abh 192:275–287

Baumgartner R, Romer RL, Moritz R, Sallet R, Chiaradia M (2006) Columbite-tantalite bearing granitic pegmatites from the Seridó belt, Northeastern Brazil: genetic constraints from U-Pb dating and Pb isotopes. Can Mineral 44:69–86

Burke EAJ (2008) Tidying up mineral names: an IMA-CNMNC scheme for suffixes, hyphens and diacritical marks. Mineral Mag 39:131–135

Černý P, Ercit TS, Wise MA (1992) The tantalite-tapiolite Gap: natural assemblages versus experimental data. Can Mineral 30:587–596

Chukanov NV, Pasero M, Aksenov SM, Britvin SN, Zubkova NV, Yike L, Witzke T (2023) Columbite supergroup of minerals: nomenclature and classification. Mineral Mag 87:18–33

Donovan JJ, Pingitore NE, Westphal A (2003) Compositional averaging of back-scatter intensities in compounds. Microsc Microanal 9:202–215

dos Santos CA, Zawislak LI, Kinast EJ, Antonietti V, da Cunha JBM (2001) Crystal chemistry and structure of the orthorhombic (Fe,Mn)(Ta,Nb)$_2$O$_6$ family of compounds. Braz J Phys 31(4):616–631

Ercit TS, Wise MA, Černý P (1995) Compositional and structural systematic of the columbite group. Am Mineral 80:1019–1028

Erlacher A, Zeug M, Škoda R, Sameera KAG, Nasdala L (2021) Metamict fergusonite from Kolonna and Masimbula, Sri Lanka. J Geol Soc Sri Lanka 22(2):1–14

Feng YG, Liang T, Linnen R, Zhang Z, Zhou Y, Zhang ZL, Gao JG (2020) LA-ICP-MS dating of high uranium columbite from no. 1 pegmatite at Dakalasu, the Chinese Altay orogen: assessing effect of metamictization on age concordance. Lithos 362–363:105461. https://www.sciencedirect.com/science/article/pii/S0024493720300980

Giuseppetti G, Tadini P (1990) The crystal structure of vigezzite, (Ca,Ce)(Nb,Ta,Ti)$_2$O$_6$, intermediate term of the aeschynite series. N Jb Miner Mh 1990:301–308

Hall MG, Lloyd GE (1981) The SEM examination of geological samples with a semiconductor back-scattered electron detector. Am Mineral 66:362–368

Hao Y, Feng Y, Liang T, Brzozowski M, Ju M, Zhou R, Wang Y (2023) Quantitative evaluation of metamictisation of columbite-(Mn) from rare-element pegmatites using Raman spectroscopy. Mineral Mag 87:337–347

Hatchett C (1802) An analysis of a mineral substance from North America, containing a metal hitherto unknown. Philos Trans R Soc 92:49–66

Hess HD, Trumpour HJ (1959) Second occurrence of fersmite. Am Mineral 44(1–2):1–8

Husson E, Repelin Y, Dao NQ, Brusset H, Fardouet E (1977a) Infrared and Raman spectrophotometric studies of niobates of columbite structure. Spectrochim Acta Mol Biomol Spectrosc 33(11):995–1001 (in French)

Husson E, Repelin Y, Dao NQ, Brusset H (1977b) Normal coordinate analysis of the MNb$_2$O$_6$ series of columbite structure (M = Mg, Ca, Mn, Fe, Co, Ni, Cu, Zn, Cd). J Chem Phys 67(3):1157–1163

Kristiansen R (1994) Two new minerals for Norway– manganocolumbite and hingganite–(Yb). Nordisk Magasin for Populær geologi. 21(2):88–93 (in Norwegian)

Kumari TSD, Gandhi RV, Rahul G, Kamalanathan G, Kumar TP, Jeyakumar D, Lakshminarasimhan N (2014) Electrochemical lithium insertion behavior of FeNbO$_4$: structural relations and in situ conversion into FeNb$_2$O$_6$ during carbon coating. Mater Chem Phys 145:425–433

Linnen RL, Van Lichtervelde M, Černý P (2012) Granitic pegmatites: granitic pegmatites as sources of strategic metals. Elements 8:275–280

Loun J, Novák M, Cempírek J, Škoda R, Vašinová Galiová M, Prokeš L, Dosbaba M, Čopjaková R (2018) Geochemistry and secondary alterations of microlite from eluvial deposits in the Numbi mining area, South Kivu, Democratic Republic of the congo. Can Mineral 56(2):203–220

Melcher F, Graupner T, Gäbler HE, Sitnikova M, Dewaele S (2015) Tantalum-(niobium-tin) mineralisation in African pegmatites and rare metal granites: constraints from Ta-Nb oxide mineralogy, geochemistry and U-Pb geochronology. Ore Geol Rev 64:667–719

Merlet C (1994) An accurate computer correction program for quantitative electron probe microanalysis. Mikrochim Acta 114/115(1):363–376

Moreira RL, Rubinger CP, Krambrock K, Dias A (2010a) Polarized Raman scattering and infrared spectroscopy of a natural manganocolumbite single crystal. J Raman Spectrosc 41:1044–1049

Moreira RL, Teixeira NG, Andreeta MRB, Hernandes AC, Dias A (2010b) Polarized micro-Raman scattering of CaNb$_2$O$_6$ single crystal fibers obtained by laser heated pedestal growth. Cryst Growth Des 10:1569–1573

Mulja T, Williams-Jones AE, Martin RF, Wood SA (1996) Compositional variation and structural state of columbite-tantalite in rare-element granitic pegmatites of the Preissac-Lacorne batholith, Quebec, Canada. Am Mineral 81:146–157

Nasdala L, Hauzenberger C, Wildner M, Chanmuang NC, Sameera KAG (2023) Metamict gadolinite–(Y) from Ratnapura, Sri Lanka. J Geol Soc Sri Lanka 24(1):23–30

Nonius (1998) Kappa CCD program package. Nonius, Delft

Prame WKBN, Edirisinghe GDN, De Silva KTUS, Dissanayake DMS (2014) Samarskite-polycrase group minerals and other radioactive minerals associated with gem gravels in the Ratnapura gem field of Sri Lanka. Proc 30th techn session. Geol Soc Sri Lanka, p 1

Ruschel K, Nasdala L, Kronz A, Hanchar JM, Többens DM, Škoda R, Finger F, Möller A (2012) A Raman spectroscopic study on the structural disorder of monazite–(Ce). Min Petrol 105:41–55

Tarantino SC, Zema M (2005) Mixing and ordering behavior in manganocolumbite–ferrocolumbite solid solution: a single-crystal X-ray diffraction study. Am Mineral 90:1291–1299

Tealdi C, Mozzati MC, Malavasi L, Ciabattoni T, Amantea R, Azzoni CB (2004) Columbite-type $Fe_xMn_{1-x}Nb_2O_6$ solid solution: structural and magnetic characterization. Phys Chem Chem Phys 6:4056–4061

Wenger M, Armbruster T, Geiger CA (1991) Cation distribution in partially ordered columbite from the Kings Mountain pegmatite, North Carolina. Am Mineral 76:1897–1904

Zeug M, Nasdala L, Wanthanachaisaeng B, Balmer WA, Corfu F, Wildner M (2018) Blue Zircon from Ratanakiri, Cambodia. J Gemmol 36(2):112–132

Ziebold TO (1967) Precision and sensitivity in electron probe analysis. Anal Chem 39:858–861